

# Temperature- and Wind-induced Air Flow Patterns in a Staircase.

## Computer Modelling and Experimental Verification

H. FEUSTEL, CH. ZUERCHER\*, R. DIAMOND, B. DICKINSON, D. GRIMSRUD and R. LIPSCHUTZ

*Energy Performance of Buildings Group, Energy and Environment Division, Lawrence Berkeley Laboratory, University of California, Berkeley, CA 94720 (U.S.A.)*

(Received August 22, 1984; in revised form November 7, 1984)

### SUMMARY

*The typical infiltration load for a residential building has been found to range from one-third to one-half of the total space conditioning load. However, most infiltration measurements have been made on single-family houses. Information about the role of infiltration in the energy consumption of large buildings is limited. Furthermore, the prediction of infiltration rates in high-rise buildings is a complex problem. The forces that drive this flow result from the superposition of wind pressure on the faces of the building and the stack effect across the height of the building. Infiltration models have shown the latter effect to be significant in single-family residences, particular in colder climates and, consequently, the stack effect is even greater in high-rise buildings. For this work, we performed tracer gas and fan pressurization measurements on a 30 m tall University of California dormitory in order to determine the importance of both wind and stack effect upon infiltration. Measured pressure and tracer gas distributions were compared with those from a predictive infiltration computer model for high-rise buildings. To study the influence of the air flow pattern around the building, this model uses various wind velocity profiles characteristic of urban areas and different sets of surface pressure coefficients derived from wind tunnel experiments.*

**Key words:** air-infiltration 'multi-cell' calculation model, thermal buoyancy and wind effect, fan pressurization, leakage area, tracer

\*Present address: Institute of Building Technology, Dept. Building Physics, ETHZ, CH-8093 Zürich, Switzerland.

gas measurements, wind pressure data and air infiltration calculation.

### INTRODUCTION

Studies on the energy consumption for the mid-seventies show that most of the industrialized countries squander a large amount of precious energy (oil, gas, coal) for low-grade thermal processes. Up to one-third of the overall primary energy is used for residential and commercial buildings [1 - 3]. Over half of this energy consumption in the building sector is consumed by space heating and cooling. This 'space-conditioning load' is caused by losses or gains due to heat transmission and by air movement due to infiltration and/or controlled ventilation. A typical ventilation load for a residential building structure representing the architectural construction mode before the mid-seventies is estimated to be in the range of 1/3 to 1/2 of its total space-conditioning load [4]. In contrast to the relatively steady process of heat transmission, infiltration is more strongly influenced by rapid changes in weather conditions. Moreover, infiltration is nonlinear, depending primarily on wind pressure and thermal buoyancy (stack effect), and therefore difficult to model.

Infiltration is an important component of the space-conditioning load, especially in houses with above-average shell thermal performance. As houses are made tighter to reduce infiltration losses, the maintenance of acceptable indoor air quality begins to be an issue of concern [5]. Balancing the competing demands of energy conservation and air quality may require a target ventilation rate for a structure. This, in turn, demands the existence of inexpensive instrumentation to

measure infiltration or a model that will accurately predict air movement in buildings [4].

Infiltration, the random flow of air through openings in the building surface, is for a single-family house largely independent of the house type and structure. This flow process is dominated by the leakage structure of the building rather than by structural type. Air flow is the consequence of pressure differences due to wind pressure and thermal buoyancy. Besides these driving forces, the infiltration rate however depends on the air permeability of the building structure and on the distribution of leakage areas throughout the building.

A prediction of the infiltration for high-rise buildings is a complex problem. The pressures that drive the flow are the result of the superposition of wind pressure that depends on the elevation and orientation and the stack effect. Recent works on prediction models for one-family houses [6, 7] demonstrate the strong influence of the stack effect on the infiltration rate. The latter is even more important for high-rise buildings because of the magnitude of the building height [8].

In this paper, in a first step, we try to model the air infiltration in a tall UC dormitory building with a computer program using a parabolic wind velocity profile and height-independent surface pressure coefficients. In a second part, we compare the computed air flow with experimental results from the 30 m tall dormitory. This comparison exposes the difficulties of using constant surface pressure coefficients and show that the building structure as well as the surrounding pattern has to be studied very carefully.

#### AIR LEAKAGE, AIR INFILTRATION AND VENTILATION

Air flow through a building shell is a combination of viscous and turbulent flow through openings and cracks. The former is proportional to the pressure difference over the envelope whereas the latter varies with the square root of the pressure difference.

Two different mechanisms are primarily responsible for natural air flow in buildings — wind pressures and buoyancy forces. Wind

flows will produce a velocity pressure field around the building. Compared to the static pressure in the undisturbed wind velocity pattern, these pressure fields are characterized roughly by regions of overpressure on the windward façade and underpressure on façades parallel to the air stream or on the leeward side of the building respectively. These pressure differences are proportional to the dynamic pressure in the undisturbed wind stream; they therefore can be represented relative to the latter using surface pressure coefficients:

$$p_{\text{wind}} = 1/2 * \rho(z, T) * v^2(z) * c_i(z) \quad (1)$$

The  $c_i$  values can be determined either from measurements on full-scale buildings or on corresponding small-scale models in a boundary-layer wind tunnel [9, 10]. The interpretation of the latter data in regard to real buildings still remains difficult [11].

Excluding thermal stratification, the vertical profile of the mean wind speed in the atmospheric boundary layer depends primarily on the surface roughness and shows an increasing velocity with height above ground, approximated by a power-law expression [12, 13]

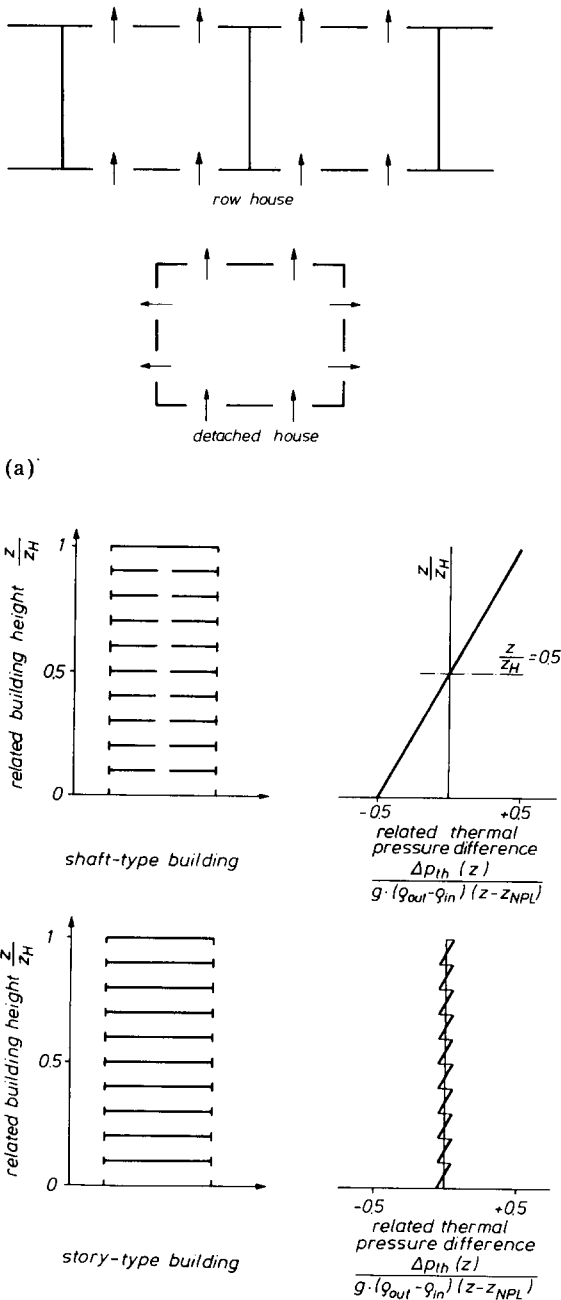
$$v(z)/v(z_0) = (z/z_0)^{1/\alpha} \quad (2)$$

Usually,  $v(z_0)$  is the meteorological reference wind speed recorded at a standard height of  $z_0 = 10$  m above ground.

Pressure gradients between inside and outside of the building also arise from changes in air density due to temperature differences between ambient air and air inside (stack effect) [14, 15]:

$$\Delta p_{\text{stack}} = g * (\rho_{\text{out}} - \rho_{\text{in}}) * (z - z_{\text{NPL}}) \quad (3)$$

with  $z_{\text{NPL}}$  as the neutral pressure level, the height on the building façade where the interior pressure equals the exterior. The influence of these thermal pressure forces are not negligible, especially in high-rise buildings [16]. At zero wind speed and air leakage distributed uniformly over the building shell, conservation of mass requires that the neutral pressure level should be at mid-height, separating the upper half of the building with overpressure from lower parts with underpressure [17 - 20]. For an extremely large opening relative to others, the above-mentioned pressure zone will be found at the



(a) Subdivision of the building type according to the permeability ratio (leakage area of the leeward windows and doors compared to the corresponding value over the total building shell). (b) Thermal pressure difference as a function of the type of construction for  $t_{in} > t_{out}$  and the air leakage uniformly distributed over the building shell.

height of the center of this opening. For air flows caused by combined action of wind and thermal buoyancy, the flows due to each

mechanism do not add, since the flow rates are not linearly proportional to the pressure differences.

Referring to infiltration, a building may be classified using one of the following four broad categories:

- (a) row house (terrace house)
- (b) detached house
- (c) story-type construction
- (d) shaft-type construction.

This subdivision into four basic cases is based on a comparison of the permeability behavior of a building as function of its location (influence of wind effect) as well as of its construction type (influence of stack effect). This classification of the house types with regard to air infiltration calculations is schematically displayed in Figs. 1(a) and (b) respectively.

The air permeability is a property of a building component/region to let air pass when it is subject to a pressure difference and can be compared to a sum over crack coefficient  $a_i$  times crack length  $l_i$  for all air openings  $i$  in the region to be specified. Under the assumption of nearly uniform distribution of the air openings over the building shell, the detached and row house differ in the ratio of the leeward side's permeability to the overall permeability ratio of the house [21]:

$$R = D_{lee} / (D_{lee} + D_{wind}) \quad (4)$$

Based on an investigation of Krischer and Beck, row houses, in a first approximation, can be described by an averaged permeability ratio of 0.5, whereas the corresponding value for a detached house rises up to 0.7. On the other hand, with regard to the thermal pressure distribution, there exist two extrema: story-type buildings and shaft-type buildings. That means one can describe the building relative to the value of the permeability of its components separating floor areas from shafts connecting the different floors (e.g., staircase, elevator shaft, etc.). With  $D_s$  as permeability of the separating building component, the construction types above can be described with

$$D_s = 0 \text{ for a story-type construction} \quad (5)$$

and

$$D_s = \text{infinity for a shaft-type building} \quad (6)$$

In a building with shaft-type construction, the influence of thermal pressure forces are extremely strong. With a uniform distribution of the permeabilities as a function of height throughout the façade- and shaft plane, the neutral pressure level zone should be at the mid-height of the building. Otherwise, its location for this construction type will be principally determined by the permeability distribution of the shaft [22]. As height and number of stories increase, the total resistance of the flow path through floor openings increases faster than through vertical shafts, so the shaft mainly governs total resistance to the flow in high buildings [8, 23]. On the other hand, in a story-type building, there are small buoyancy effects only within every floor. Every story, depending on its permeability distribution, will have its particular neutral pressure level zone. Existing houses can now be described within these four broad categories, e.g., to get an estimation for the upper value of the air infiltration in a house to be constructed. Such considerations, especially if they are supported by tables taking into account different building heights, weather conditions etc., are a helpful tool for designers of heating plants and systems [8, 24]. For more accurate results, one has to establish complex computer programs with mass flow balances considering all possible flow paths in a building.

## EXPERIMENTAL TECHNIQUES

### *Building and climatological survey*

The four dormitories comprising Unit I of student housing for the University of California at Berkeley occupy a 0.9 ha site two blocks south of the campus. The surrounding blocks are mostly three-story residential apartments, with the University Museum to the north and an athletic playing field to the south. The dorms are identical nine-story buildings, arranged on the periphery of the block, oriented both north/south and east/west (see Fig. 2(a)).

The buildings were constructed in 1960 following an architectural competition run by the University. Each building is 9.75 m × 38.9 m in plan and 29.1 m in height. The ground floor is divided into an entrance

lobby, lounge, library, maintenance rooms, and a single elevator and stairwell to the roof (Fig. 2(b)). The height of the ground floor is 4.9 m; the upper stories are all 3 m floor-to-floor. The stairwell (9.75 m<sup>2</sup>) is located on the east wall. A steel-framed single-glazed window (2.2 m<sup>2</sup>) is located on the landing level between each floor (Fig. 2(c)). The elevator shaft (5.2 m<sup>2</sup>) is adjacent to the stairwell. The upper floors have student rooms (16.9 m<sup>2</sup>) along both sides of a single corridor leading to an exterior stair tower. Each floor has a common bathroom and either a lounge or a laundry (Fig. 2(d)). The structure is reinforced concrete with metal curtain walls and cast stone grills on the exterior wall of the utility rooms.

With Berkeley located on the east shore of San Francisco Bay, the climate is characterized by mild year-round temperatures and prevailing westerly winds from the Pacific. Vicarious, averaged temperatures, degree-days and wind parameters from the nearby Oakland Airport are shown in Table 1.

### *Blower-door measurements*

The pressure-flow characteristics for the different leakage locations were measured using a door-mounted, variable-speed fan capable of moving large volumes of air into or out of a structure. When the pressure difference ( $\Delta p$ ) is held constant, following the law of constancy of mass, all air pressed through the fan must flow through the building structure to be measured. Natural infiltration is typically driven by pressure differences across the building shell in the range of 0 Pa to 10 Pa and is characterized by large, short-term fluctuations. When  $\Delta p$  is much greater than 10 Pa, fan flow dominates natural infiltration and the latter may be disregarded. At a given  $\Delta p$  and a fan speed, the flow of air is determined by means of a previously established calibration curve. With the aid of measurements at discreet  $\Delta p$ 's in the over- as well as underpressure region (−70 Pa to +70 Pa), the parameters  $D$  and  $n$  are fitted to the following equation characterizing the air flow through a leaky building shell:

$$\dot{Q}(\Delta p) = D * (\Delta p)^n = \dot{Q}_{fan}(\Delta p) \quad (7)$$

The flow exponent  $n$  of the pressure difference across the opening ranges in value between 0.5 for fully turbulent flow to 1.0 for

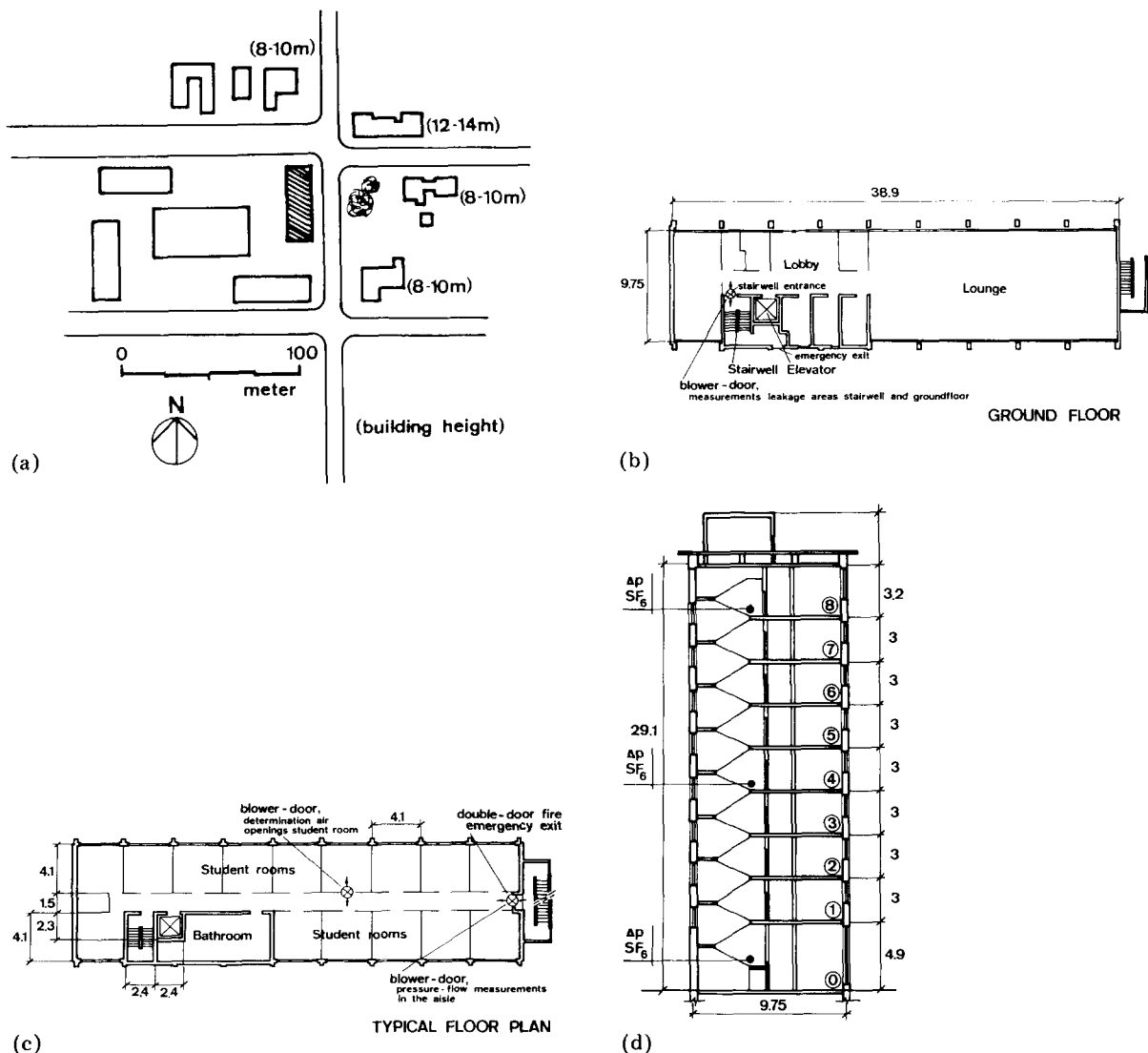


Fig. 2. (a) Building location, (b) ground-floor plan, (c) typical floor plan, and (d) staircase section.

TABLE 1

Climatological data for Oakland

	Jan	Feb	Mar	Apr	May	Jun	Jul	Aug	Sep	Oct	Nov	Dec
<b>Temperature (°C)</b>												
average monthly	9.2	11.1	12.1	13.4	14.9	16.6	17.3	17.5	18.1	16.2	12.9	9.9
average daily max.	12.8	14.4	15.6	17.2	18.3	20.6	21.1	21.1	22.2	20.6	16.7	13.3
average daily min.	6.1	7.8	8.3	9.4	11.1	12.8	13.3	13.9	13.9	11.7	9.4	6.7
<b>Degree-days</b>												
heating												
(18.5 °C base)	508	367	350	270	193	114	80	74	59	135	291	468
cooling												
(18.5 °C base)	—	—	—	—	—	21	21	28	44	14	—	—
<b>Wind</b>												
mean speed* (m/s)	3.0	3.3	4.0	4.2	4.5	4.5	4.2	4.0	3.5	3.0	2.8	2.9
prevailing direction	SE	W	W	W	W	W	WNW	WNW	WNW	WNW	WNW	E

\*meteorological wind speed at 10 m above ground:  $u(10)$ .

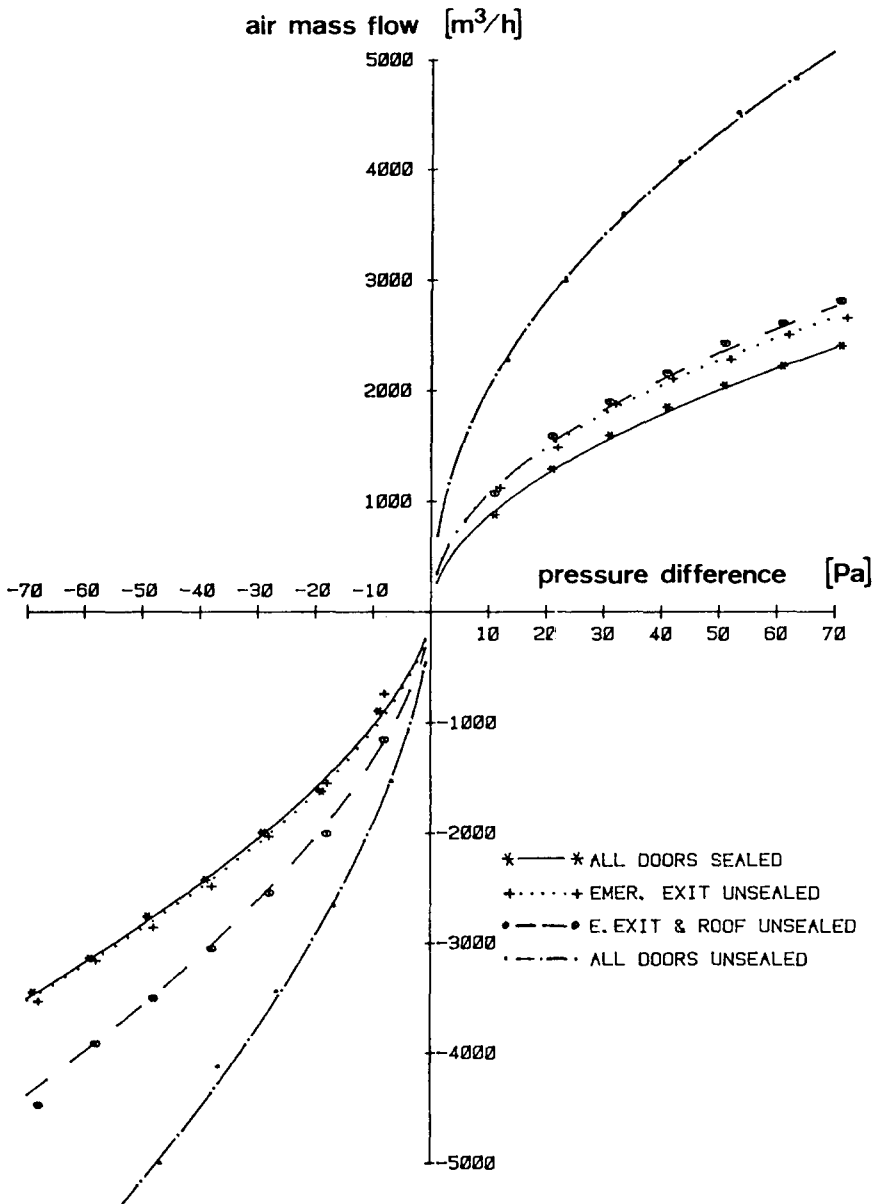


Fig. 3. Pressure-flow characteristics in the stairwell.

laminar streams, regardless of the Reynolds number [6]. For rough estimates one usually assumes an averaged flow exponent of 2/3.

Figure 3 demonstrates the different pressure-flow regimes in the stairwell due to changes in leakage area by opening previously sealed air cracks.

Table 2 lists the air flow parameters  $D$  and  $n$  for the different leakage areas of the building. Using weighting factors taking the higher uncertainty of the measurements at low pressure differentials into account, correlation coefficients between 0.97 and 1.0 pointed at a good agreement between the fitted curve and the measurements.

Strictly speaking and especially for an accurate determination of the low pressure leakage function (0 - 10 Pa) blower-door measurements should be performed under climatic conditions without temperature differences across the construction elements due to wind flow characteristics. If an individual space is being pressurised, all adjoining spaces (lateral as well as vertical) must be at a similar pressure to measure the leakage characteristic of the exterior wall. If not, internal leakages will also be included in the result. On the other side, the flow characteristic of a particular construction component can be determined from the differences in

TABLE 2

Air leakage parameters for different structure parts, determined from blower-door measurements

Boundary conditions	Pressurization		Depressurization	
	$D$ ( $\text{m}^3/\text{Pa}^n\text{h}$ )	$n$	$D$ ( $\text{m}^3/\text{Pa}^n\text{h}$ )	$n$
Stairwell				
all doors sealed	262	0.52	241	0.63
emergency exit unsealed	362	0.47	264	0.61
emergency exit and roof door unsealed	345	0.49	323	0.61
all doors unsealed	690	0.47	456	0.62
Ground floor				
all internal doors sealed incl. elevator	608	0.57	370	0.69
all internal doors unsealed, elevator sealed	609	0.59	381	0.71
all internal doors open, elevator sealed	737	0.60	450	0.74
all internal doors sealed, elevator unsealed	628	0.62	411	0.72
Student room	36	0.75	29	0.79
1st floor aisle				
all doors closed, elevator sealed	473	0.63	411	0.66
all doors closed, elevator door unsealed	794	0.54	518	0.64
1st floor lounge	54	0.72	69	0.70

volumetric air flow using selective sealing of components.

#### Tracer gas and pressure measurements

The air flow in the stairwell was experimentally determined using a tracer gas technique. Injecting  $\text{SF}_6$  at the ground floor at a constant flow rate, its concentration at the 1st, 4th and 8th floor were recorded together with pressure differences (ground floor and 8th floor) and temperatures as a function of time. Due to the large molecular weight of  $\text{SF}_6$  (146 g/mol compared to the averaged value of 29 g/mol for air), the tracer gas was uniformly mixed with the atmosphere at the ground floor using a fan. Therefore, stratification due to settling out of the heavier gas should be unlikely [25]. The flow rate was kept constant by the use of an electronic mass flow controller based on the principle of heat transfer by the tracer gas along a capillary. Using the continuity equation for a constant tracer gas flow rate

$$C(t) = F/\dot{Q} + [C(t_0) - F/\dot{Q}] \exp[-\dot{Q}/V * (t - t_0)] \quad (8)$$

the tracer gas concentration at the ground-floor level will reach steady-state levels of 10 ppm or 15 ppm for estimated volumetric air infiltration rates of 300  $\text{m}^3/\text{h}$  and 200  $\text{m}^3/\text{h}$  respectively and a constant flow

rate of about 50 ml/min. Multiple sampling throughout the stairwell cross section provided properly averaged measurements of the  $\text{SF}_6$  concentrations at the selected floor levels. Based on infrared properties of sulfur hexafluoride, the tracer gas concentration itself was calculated from measurements of the transmission losses in a 1.5-m gas cell of 2.5  $\text{dm}^3$  at 10.7  $\mu\text{m}$  with an optical vapor analyzer. For gas concentrations between 0 ppm and 15 ppm, calibration runs with up to 20 different sampling points were carried out in order to fit the analyzer output voltage with the aid of a simplex algorithm to an exponential function, taking into account the concentration-dependent absorption power of the tracer gas. The accuracy in the determination of the gas concentration is estimated to about  $\pm 13\%$ .

A capacitive potentiometer with a thin, prestressed metal diaphragm as variable, sensitive element was used as differential pressure sensing element.

#### Computer modelling of the air flow in a high-rise building

The calculation of natural ventilation rates in a building is a complex task. Several methods exist at the present — one estimation procedure known as the 'crack method' is based on measured air leakage rates of building components [e.g., 23, 24], another

assumes air change numbers for the different building sections [e.g., 23, 26]. Contrary to full-scale techniques, several authors have developed air infiltration prediction programs using detailed surface mean pressure coefficients measured in wind tunnel experiments [27 - 30]. One other technique applying the theory of electrical networks to the flow system, faces the problem that the pressure-flow characteristics across air openings are nonlinear in contrast to the voltage drop across a resistance due to electrical current flow [31, 32].

Simulation programs using an iteration method are normally based on a network containing a large number of nonlinear equations. Therefore the only useful tool to get a solution is a computer [33]. According to the most common applications, the computer programs solve generally for one-family houses [e.g., 34 - 36]. Programs able to simulate air flows in buildings with up to 200 rooms are available at the NRC of Canada [37], BSRIA in Great Britain [38] and the HRI in Germany [22].

The latter routine, which is the framework for the computer model used in this study, calculates solutions of its nonlinear equation system using Newton's iteration method. With floors, stairwell and elevator shaft represented by a series of rooms, each at a specific pressure and temperature, the movement of air through the building will be computed by a program based on steady-state pressure dependent mass flow balances at each floor as well as in the two shafts (elevator shaft and stairwell). The net mass flows between ingoing and outgoing air through the air openings of the  $r$ -th surface are calculated by:

$$\dot{m}_r = \rho * D_r * (\Delta p_r)^{n_r} \quad (9)$$

The permeabilities  $D_r$  and the flow exponents  $n_r$  will be determined from blower-door measurements. At the location of the different air openings, the wind-induced pressure field around the building was calculated using eqn. (1), with wind velocities depending on the height above ground as in eqn. (2). On the windward side, the mean surface pressure coefficient was set to be 1, whereas on the leeward side the corresponding value was estimated to about  $-0.3$  [21]. In the exponent of the power law for the vertical wind

velocity profile above ground (eqn. (2)),  $\alpha$  was chosen to be 3 as an averaged value for urban areas [39]. The pressure differences caused by stack effect are calculated in agreement to eqn. (3). To limit the input data for the simulation program and to save cost-causing calculation time, we have simplified the floor plans of the building. For wind directions perpendicular to a main building façade, the wind pressure at a specified height will normally be idealized by width-independent pressure coefficients for each surface orientation (compare Fig. 21 in [4]). Therefore, at each floor, all rooms with equal door and window permeabilities and the same orientation as for the façade, can be mathematically treated as one room. Since permeabilities are additive like conductances in an electrical network, such a simplified room can be attached to a resulting permeability. Hence, the flow resistance for a window and a door located in series as, for example, in the student rooms will be calculated to

$$Z = D_{(\text{tot})}^{-1} = [D_{(\text{window})}^{-1/n} + D_{(\text{door})}^{-1/n}]^n \quad (10)$$

In the building to be investigated, a story containing all student rooms, lounge/laundry and aisle, except the corresponding portions of the stairwell and elevator shaft, can be described by substitute resistances related to each façade. Table 3 roughly summarizes the input data used for the computer modelling of the dormitory.

The following Figures will outline principal results obtained from the calculations of air flow patterns in the building and pressure differences across the construction as a function of different weather conditions. Considering the net ingoing air flow for the entire building without referring to any special building surface, at 0 m/s wind speed and an averaged ambient air temperature of 13 °C (compare Fig. 4), there will be no additional energy requirement in the building to compensate 'cold' air infiltration except for stories lower than the 6th floor.

With increasing wind speed the shape of the ingoing air flow curve will be more and more influenced by its power-law velocity profile. It is remarkable that the air flow at the ground floor will not be influenced by changes in wind speed. For the same weather condi-

TABLE 3

Parameters used for computer modelling of the air flow in the dormitory (first calculations with constant surface pressure coefficients)

Wind direction	east
Wind speed: $v(10)$	0 to 6 m/s
Ambient air temperature	-15 °C to +20 °C
Indoor air temperature aisles (floor level)	17.5 °C (0), 21.0 °C (1), 20.0 °C (2), 18.5 °C (3), 17.5 °C (4), 17.0 °C (5), 17.0 °C (6), 18.0 °C (7), 18.3 °C (8)
staircase	21.0 °C
elevator shaft	19.0 °C
Wind velocity profile	power law (eqn. (2)) with $\alpha = 3.0$
Surface pressure coefficients windward side	+1.0
sides, leeward side	
roof	-0.3
Permeabilities $D_r$ and flow exponents $n_r$	See Table 2, east and west façade values from depress- and press blower-door measurements respectively; the 8th floor stairwell window showed a leakage area about 2 to 3 times higher than the corresponding value for the other levels.

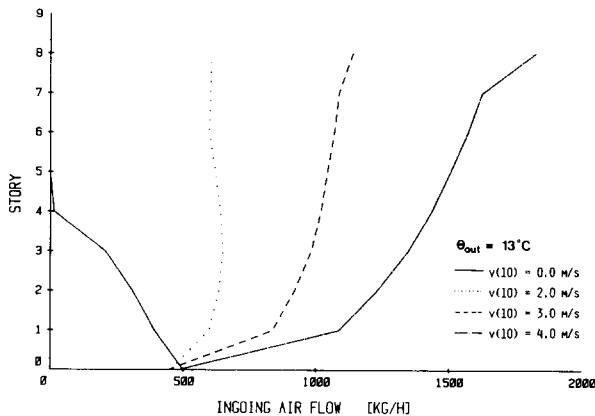


Fig. 4. Influence of the wind velocity on the air flowing into the building ( $\theta_{out} = 13$  °C).

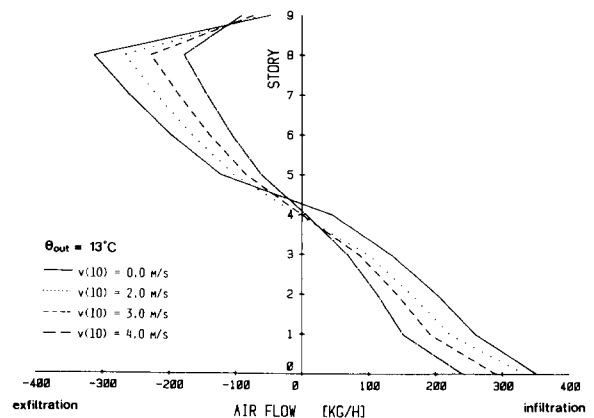
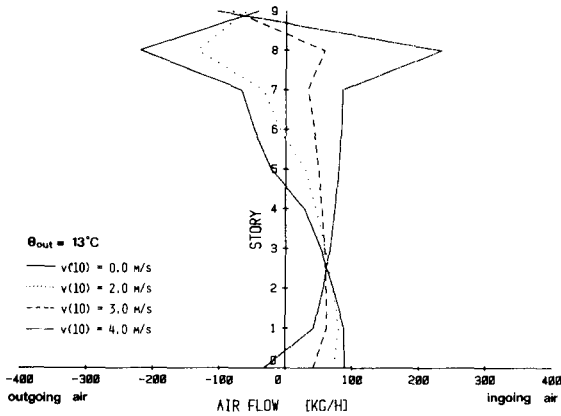


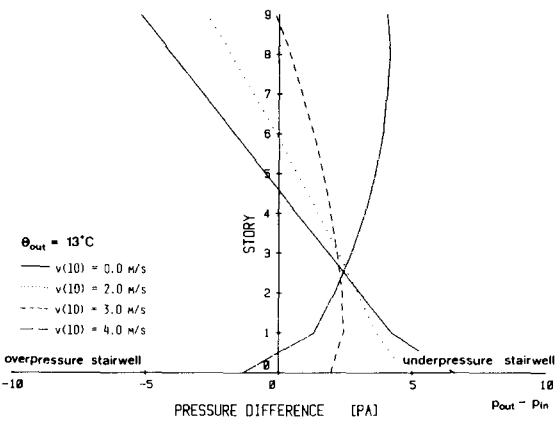
Fig. 5. Air flow through openings of the elevator shaft for different wind speeds ( $\theta_{out} = 13$  °C).

tions, Figs. 5 to 8 display the flow regimes in different selected building parts. Independent from wind speed, in the elevator shaft air from floors below the 5th level flows to the shaft, whereas the emanation of air from higher levels increases to its maximum at the 8th floor. Therefore, as a consequence of conservation of mass, an air current in the elevator shaft will transport ground-floor air to higher levels. Such an air exchange in the building may have undesired accompaniment such as the transport of air pollutants like airborne bacteria and viruses in hospitals [40] or as the transport of odors in apartment houses [16]. Moreover, for the safety of occupants, such studies are a helpful tool to estimate the smoke movement in a building during a supposed fire [31].

On the other side, the air flow in the staircase demonstrates a quite different behavior. To study this flow regime, we plotted the calculated data for both the air flow from the staircase through the windward(outside) wall air openings and the air current on staircase-adjoining floors. Figures 6(a) and (b) show the air flow throughout the staircase windows including the emergency door at the ground floor and the penthouse door and their driving pressure differences respectively. The flow regime in this part of the building is governed on one side by air flowing into the structure at lower levels and on the other side, with increasing wind speed, by a decreasing air loss at higher levels. The neutral air flow level therefore rises up with increasing wind velocity. Higher



(a)



(b)

Fig. 6(a) and (b). Computer calculated in-/exfiltration flows from the staircase through air leakages in the outside surface of the building (a) and their driving pressure difference forces  $\Delta p = p_{out} - p_{in}$  (b) as function of the building height ( $\theta_{out} = 13^\circ\text{C}$ ).

wind forces at the façade due to wind speeds larger than about 3 m/s will press ambient air into the staircase, even at the top of the building. This additional air flow increases the inside pressure to such a degree that the ground-floor staircase pressure will even exceed the outside pressure at this height, leading to an outflow of air.

For the different levels, the amount of air blowing from the corridors into the staircase is plotted in Fig. 7. Higher wind speeds cause air flows from the shaft into the corridors through all staircase doors, whereas at wind speeds smaller than 2 m/s indoor air from the student rooms and the corridors is pressed into the shaft only at lower levels.

Referring to Figs. 6 and 7, one will establish, that at wind speeds higher than about 3 m/s, the air current through the staircase door at the bottom of the building starts to change its

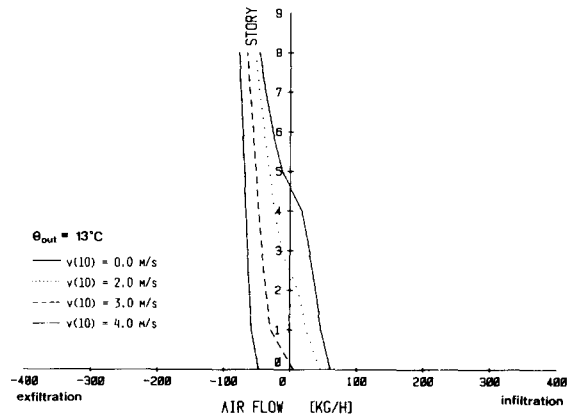


Fig. 7. Wind effect onto the air current from the corridors to the staircase at different floor levels ( $\theta_{out} = 13^\circ\text{C}$ ).

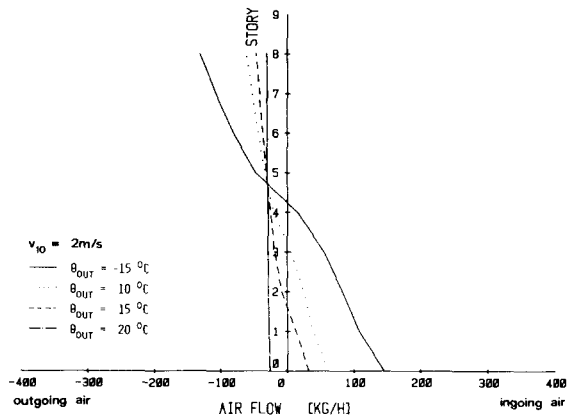


Fig. 8. Influence of ambient air temperature changes onto the air flow to the staircase from different floors ( $v_{wind} = 2\text{ m/s}$ ).

flow direction. Therefore, air pours forth through all leakage areas at the ground floor. Furthermore, according to Fig. 7, there will be no air exchange between the different floors through the staircase.

The following set of plots discusses the air mass flow in selected building areas as a function of the ambient air temperature for an averaged wind velocity of 2 m/s (Figs. 8 and 9). For the flow regime through the corridor doors of the staircase, the stack effect for a temperature gradient indoor to outdoor of about  $35^\circ\text{C}$  causes at lower levels a high air intake from the floors to the staircase (Fig. 8). The zero flow level is close to the 5th floor. With decreasing temperature difference, the ingoing air flow at the ground floor decreases too and the neutral flow level for this surface of the staircase shifts towards the ground level.

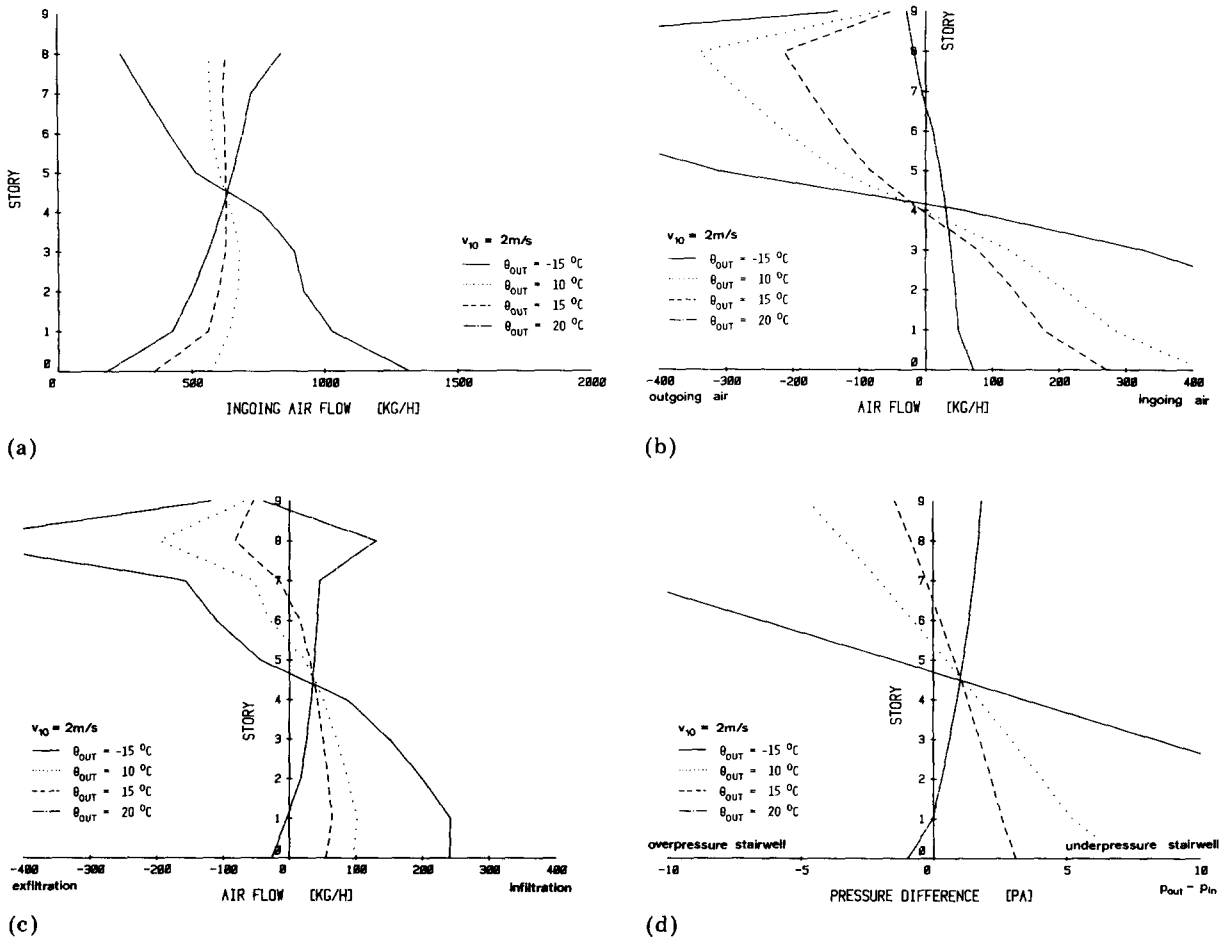


Fig. 9. Temperature and height dependence of: (a) total air flow into the building; (b) air current through elevator shaft doors; (c) air flow through openings in the outside surface of the staircase; (d) pressure differences between windward building façade and staircase (wind speed:  $v(10) = 2 \text{ m/s}$ ).

The temperature dependence of the net air flow throughout the whole structure demonstrates a well-known phenomenon for low temperatures (Fig. 9(a)). Especially in areas characterized by low winter temperatures, the overall energy demand for a heating period to equal the ventilation heat load at the ground floor of a six-story building due to natural ventilation will be at least 2.5 times higher than the equivalent amount needed to heat the top floor [41]. In our building, at an outdoor temperature of  $\theta = -15 \text{ }^\circ\text{C}$  the above-mentioned ratio will rise up to 5.5. On the other hand smaller temperature differences lead to a more balanced air current as a function of building height. But even for the building under investigation located in an area with mild year-round temperatures, there will be a remarkable ‘energy deficit’ in winter time due to cold ambient air streaming into the

lower levels and warm indoor air pressed out in the upper half of the structure.

This example clearly shows, that apart from the influence of radiation processes on the energy consumption of buildings [42], the space conditioning due to natural ventilation losses calls for a very sensitive control of the room heating system. Especially in the building investigated, the steam heating system seems to be unable to cope with this problem inducing the inhabitants of this student housing to control the room temperature individually i.e., by opening the windows.

COMPARISON – MODEL AND MEASUREMENTS

*Wind and surface pressure coefficients*

Since there exists no mathematical expression to calculate accurately the air flow

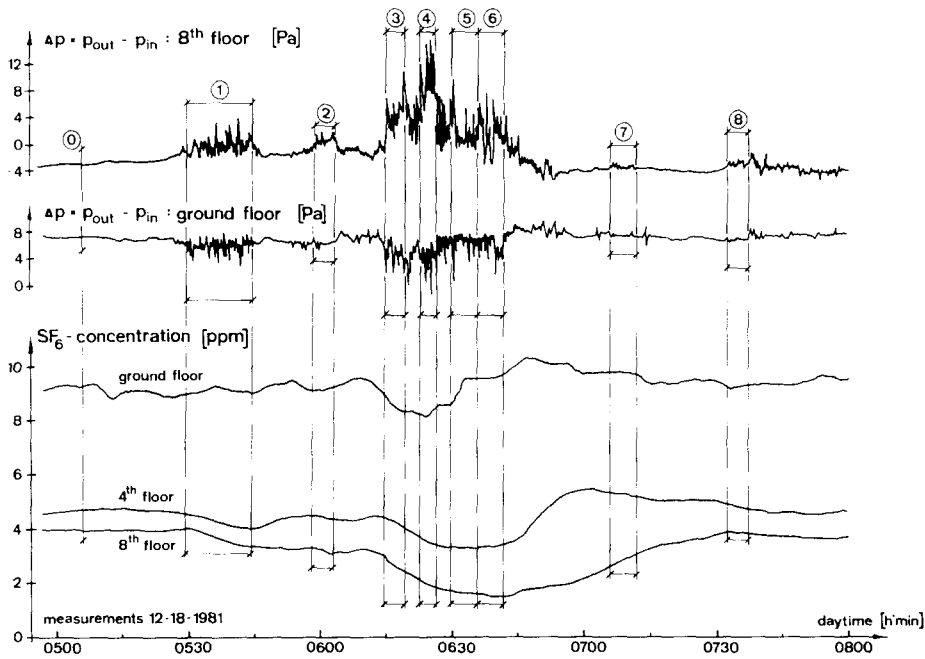


Fig. 10. Extract from pressure and tracer gas measurements at the dormitories, average outside temperature  $\theta_{out} = (12 \pm 1)^\circ\text{C}$ .

pattern around a building, the latter is still difficult to predict and changes for the same building shape from location to location due to the influence of nearby structures. In our calculation model we used a simplified surface pressure distribution based on the power-law dependence for the wind velocity profile in the atmospheric boundary layer over urban areas with constant surface pressure coefficients for each surface. The flow pattern in front of the windward façade will be strongly affected by upstream structures. This streamline pattern striking the front of a tall building will be divided in an upwind flow at higher levels and a lower region governed by downstreaming wind, both separated by a stagnation zone. The second one separates from the building façade before reaching the ground level, creating a standing vortex near ground with sometimes high internal wind velocities. Therefore, especially near ground level, the wind pressure pattern has to be examined very carefully.

Before discussing the tracer gas measurements we outline the difficulties using height-independent surface pressure coefficients. A first comparison showed that the pressure differences measured at the ground floor and 8th floor level (see Fig. 10) cannot be explained by our previous and rough calculations.

Based on this outcome, in a first step, an arbitrary modification of the wind velocity profile taking into account higher wind pressures near the ground ( $0\text{ m} < z < 10\text{ m}$ ) led to a much better agreement but was still not satisfactory. Calculations with averaged pressure coefficients from Akins *et al.* [43] and ASHRAE Fundamentals [44] based on a reference wind velocity measured at the roof level as well as height-dependent surface coefficients from Jackman and Tech [45] even led to increasing pressure differences ( $p_{out} - p_{in}$ ) for both levels — ground floor as well as 8th floor — with increasing wind velocities (compare Fig. 11).

Only a critical analysis of the built environment and the application of boundary-layer wind tunnel results from Hussain and Lee [9] yielded satisfactory results over the whole observed wind speed range. These authors have studied the surface pressure profiles on a high building located in different upwind patterns and as a function of various height ratios (central building height compared to the average height of the surrounding structures). Since there exists no experimental values for a staggered pattern of about 18%, corresponding to the upwind built-up area in front of the dormitory, we took average values from 12.5% and 25% staggered pattern experiments at a height ratio of 3. In such a

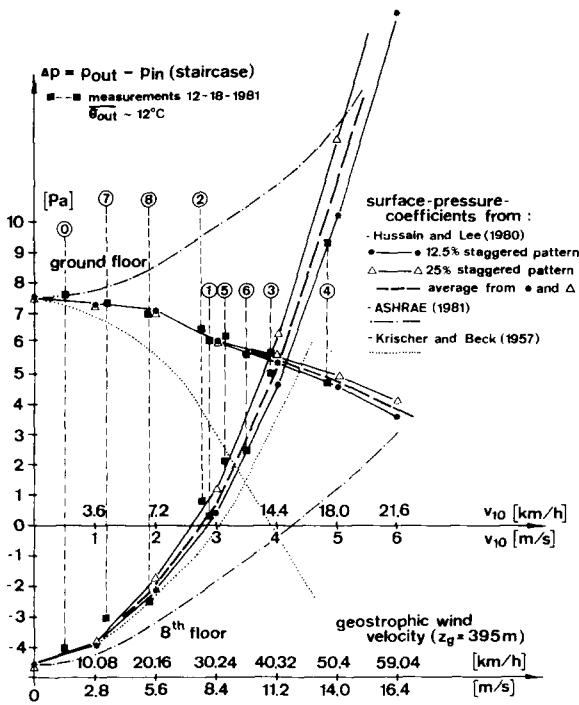


Fig. 11. Comparison of the calculated pressure differences at the ground floor and 8th floor for different surface pressure profiles.

way it was possible to correlate pairs of measured pressure differences in the wind velocity range of 0 km/h to 18 km/h at 10 m above ground. Figure 12 compares the different wind pressure profiles used in this study.

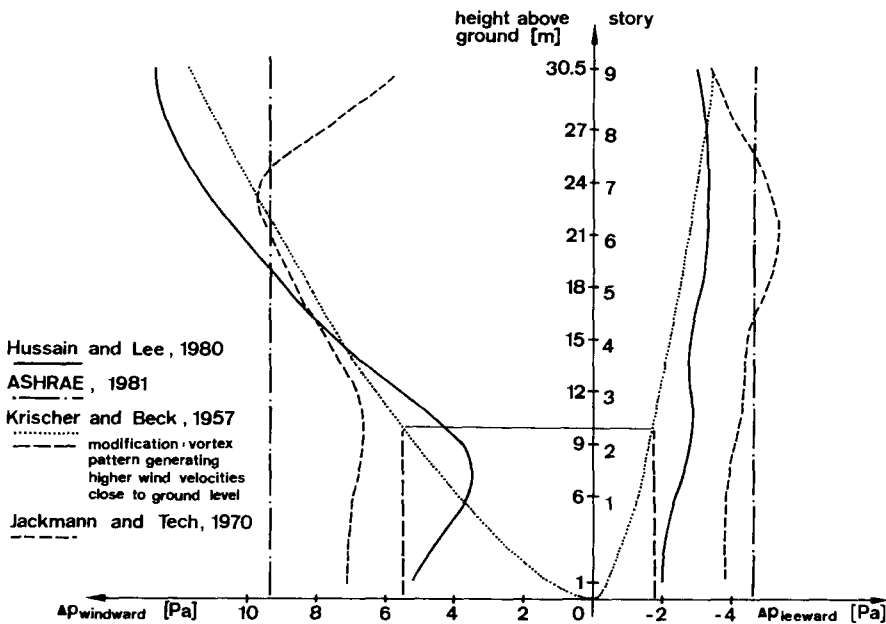


Fig. 12. A summary of the different wind pressure profiles used in this computer simulation study ( $v_{wind} (10\text{ m}) = 3\text{ m/s}$ ).

This, as well as Fig. 11 clearly demonstrate the discrepancy between the over-hasty application of simplified and constant surface pressure coefficients combined with wind velocity values describing the flow regime in an urban area.

Contrary to ASHRAE Fundamentals [44], representative average surface pressures — even combined with a questionable correction for the lower wind velocities near ground level — seem not to be the right tool to calculate air in-/exfiltrations in taller buildings.

*Tracer gas measurements*

The distribution of the tracer gas throughout the staircase during the first hours of the experiment is shown in Fig. 13. From the concentration profile at the ground floor we extrapolate a mixing time of about 1 h to 1.5 h at a gas injection rate of  $(47.5 \pm 1)\text{ cm}^3/\text{min}$ . Approaching first a maximum level near 12 ppm, the steady-state concentration at the ground floor levels out at 10.5 ppm. The overflowing in the first 3 hours can be explained by low winds pressing air in the staircase and changing the pressure distribution (compare Fig. 6(b)) so that the air exchange rate at the bottom of the building will be lowered.

Fitting the tracer gas equation (eqn. (8)) to the measured SF<sub>6</sub> concentration curve with

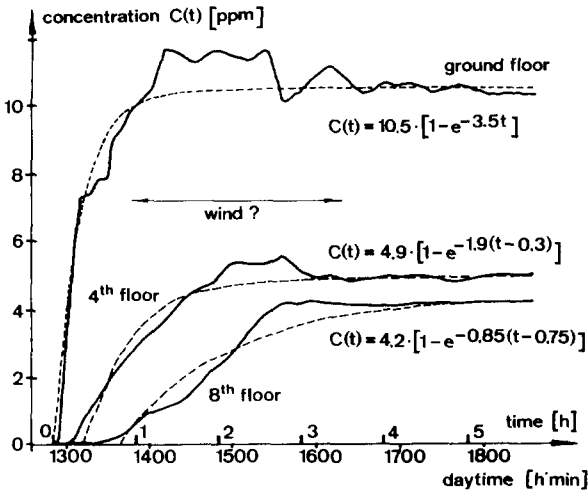


Fig. 13. Initial tracer gas concentration in the stairwell.

the aid of an inductance variation, we can extrapolate for calm weather conditions an air exchange rate at the ground floor of the staircase of  $3.5 \text{ h}^{-1}$  and an effective space volume of about  $75 \text{ m}^3$ . The latter is about two times larger than the expected physical volume of space at the injection place. This discrepancy can be explained either by the attached stairwell space communicating with the injection anteroom or by a non-recognized significant nearby air leakage participating in the air exchange and thus increasing the effective volume. On the other side, together with an approximated physical space volume of  $30 \text{ m}^3$  for the two anterooms of the stairwell (entrance from the lobby and through the rearward ground-floor emergency door), we estimate an air flow of  $105 \text{ m}^3/\text{h}$  from the ground floor to the first floor. This

estimation agrees well with the computed value in Fig. 14. Regarding the mixing times, the ground-floor  $\text{SF}_6$  concentration calculated by the fitted tracer gas equation reaches after 50 min 95% of the equilibrium concentration. The parameter matching for the time behavior of the  $\text{SF}_6$  concentration at the 4th and 8th story shows a time delay of the 'theoretical' onset of the gas mixing of 19 min and 45 min respectively.

The tracer gas measurements (Fig. 10) prove the following behaviour: with increasing wind speed, the  $\text{SF}_6$  concentration at the ground floor shows a slowly increasing trend up to a wind speed of  $4 \text{ m/s}$  to  $5 \text{ m/s}$  where the gas content decreases due to outside air which is pressed down through the staircase. Also at the 4th and 8th level we observe the same behavior but already at lower wind speeds because the flow regime at higher levels is much more influenced due to higher wind pressures on the building. A summary of the calculated air mass flow in Fig. 14 clearly demonstrates how the flow regime, dominated by the stack effect at low speeds, changes over to a reversed situation, where, principally due to wind effect a lot of air is pressed into the building through the windward air leakages at the upper levels and pours out at lower stories. At a wind speed of about  $3 \text{ m/s}$  a homogeneous intermediate state is built up where air is pressed into the building along the whole windward façade and no air flow downwards in the staircase can be observed.

For wind speeds  $v_{10}$  lower than  $3 \text{ m/s}$  only small changes in the tracer gas concentration

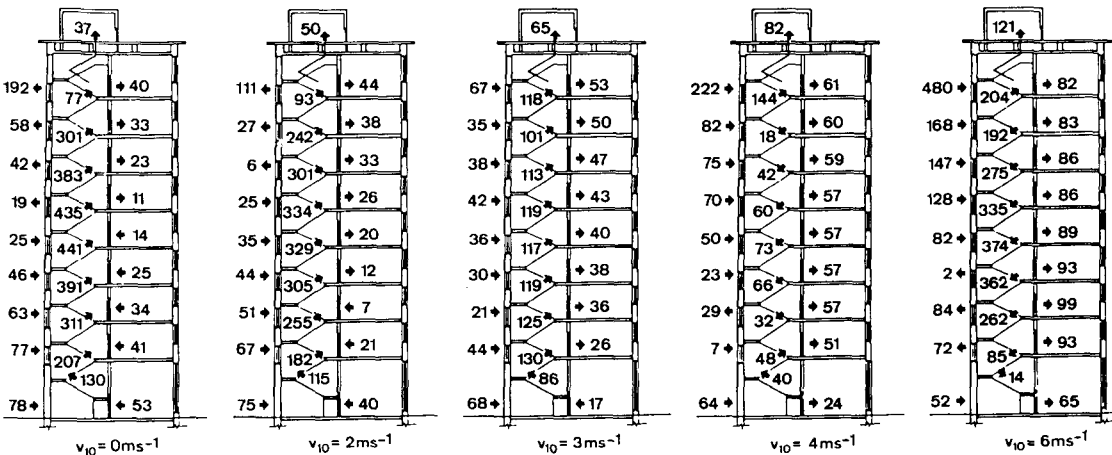


Fig. 14. Air mass flow ( $\text{m}^3/\text{h}$ ) throughout the stairwell for wind speeds  $v_{10}$  of up to  $6 \text{ m/s}$ ,  $\overline{\theta_{out}} \sim 12 \text{ }^\circ\text{C}$ .

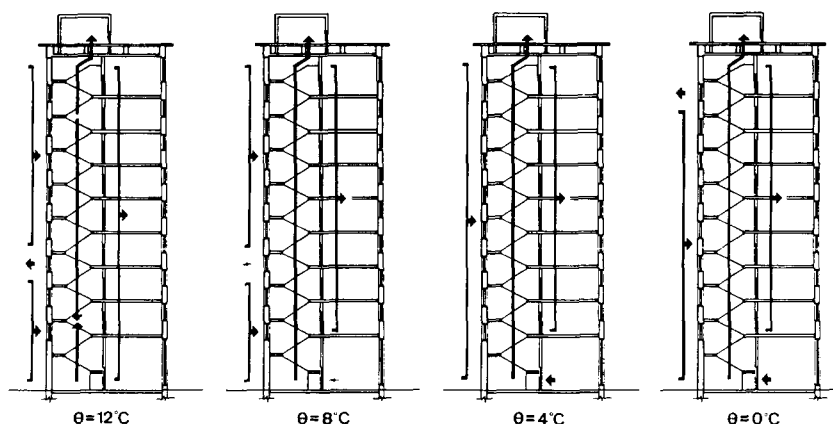


Fig. 15. Air flow pattern in the staircase for different ambient air temperature (12 °C, 8 °C, 4 °C, 0 °C) and a wind velocity of  $v_{10} = 4 \text{ ms}^{-1}$ .

at the different test levels were observed (Fig. 10, period 0, 1, 2, 7 and 8). The latter values are according to order in agreement to the  $\text{SF}_6$  content estimated from the computed air mass flows. Referring to Fig. 14 the flow regime at the 4th floor changes from upwards to downwards at wind blowing with 3 m/s to 4 m/s (compare e.g., end of period 1 in Fig. 10). With increasing wind pressure matching the measuring periods 3 and 4, all gas concentrations show a decreasing trend, also the ground-floor value. This is due to the change in the air flow direction in the stairwell between story 0 and 1 in the wind speed range of 4 m/s to 6 m/s. With less wind in the following observation intervals, the  $\text{SF}_6$  concentration at the injection place starts to increase whereas the adequate values in agreement with the flow situation represented in Fig. 14 still slowly decrease. Meanwhile the ground-floor  $\text{SF}_6$  level shows an increasing trend, the tracer gas content for the 4th level stays nearly constant due to the change in the direction of flow around 3 m/s to 4 m/s, but still decreases at the 8th floor because at every floor air containing  $\text{SF}_6$  is lost into the aisles (period 5 and 6). The last regime only changes when the wind pressure collapses and the buoyancy behavior for low wind speeds starts to be dominant in the staircase.

Besides wind effect on the air flow through the staircase, we also simulated air flow patterns with varying thermal buoyancy forces, i.e., for different ambient air temperatures down to 0 °C. With 12 °C outside air temperature, the neutral pressure level at the 5th floor with zero wind speed rises slowly to reach the top floor with about 3 m/s wind. At

this temperature, the air flow pattern in the staircase is dominated by a change in vertical flow direction at wind speeds of 3 m/s to 4 m/s (lower speeds: air flow from bottom to top; higher wind speeds: reversed direction). The lower the outside temperature drops, the longer the thermal buoyancy effect will dominate the wind effect. At 0 °C outside temperature and 4 m/s wind velocity, inside and outside pressure will be equalized between 7th and 8th floor. The vertical flow direction now will only be reversed at wind velocities between 4 m/s and 6 m/s.

## CONCLUSIONS

According to the various surface pressure profiles used in this study strongly different flow patterns in the staircase were the result. Although the total air infiltration is relatively independent of the type of pressure profile, the particular air flows throughout the building structure will be strongly affected by internal pressures as well as by the pressure distribution along the differently oriented building surfaces. Therefore, for air infiltration computer simulation and possible energy savings deduced therefrom, it is important to know — besides location and size of the air openings — the actual pressure distribution along building façades. The latter can only be done by using local pressure coefficients from wind tunnel experiments matching the natural wind velocity profile as well as the surrounding building pattern as close as possible.

Today, the characteristics of natural wind are well understood, but the local influences of surrounding topography are difficult to predict. Pressure coefficients based on wind tunnel experiments performed on isolated building shapes are widely available but may not be applicable to buildings shielded by local obstructions. More, most of today's available pressure coefficients from building codes have been evaluated from the point of view of wind loading problems, i.e., for higher wind speeds. But for air infiltration purposes low wind speeds are of interest and therefore turbulences and pressure fluctuations may be another important factor influencing the air flow pattern in a building. The accuracy of approved 'multi-cell' air infiltration simulation methods will be significantly improved if data sets of 'low-wind' pressure coefficients for fixed degrees of shielding and different building sizes are available.

Besides pressure coefficients, the wind direction proved to be a key parameter too. Therefore, to study wind-induced air infiltration problems, distribution of wind velocity and wind direction for representative weather periods are needed.

On the other hand, the need for easy-to-handle examination procedures in building standards asks for more simplified calculation methods, e.g., the application of constant surface pressure coefficients combined with a wind velocity profile modified at lower levels and at the edges of the roof taking into account the environmental wind pattern as well as the upwind landscape structure.

In the future, more research will also be needed in

— transport mechanisms in the building itself (e.g., air movement room to room with large openings; convective air flow)

— air infiltration in adjoining rooms of the same building showing different heights and orientations

— local air change rates in industrial and warehouse buildings consisting of a large single space or a small number of large spaces with or without mechanical ventilation systems.

Concluding, improved 'multi-cell' computer methods for air infiltration calculation will be a valuable tool to

— plan HVAC systems

— examine planned ventilation systems on air

flows of undesirable air pollutants (e.g., airborne bacteria and viruses in a hospital or odors in a large apartment building)

— study fire safety concepts from the point of view of smoke movement.

#### ACKNOWLEDGEMENTS

This work was supported by the Assistant Secretary for Conservation and Renewable Energy, Office of Building Energy Research and Development, Building Systems Division of the U.S. Department of Energy under Contract No. DE-AC03-76SF00098.

We gratefully acknowledge the assistance we received during the course of this work, in particular from B. Smith for his competent support in computer technical problems. The manuscript was kindly reviewed by P. Cleary and W. Nazaroff.

#### NOMENCLATURE

$a_i$	crack coefficient of the $i$ -th component ( $\text{m}^3/\text{hmPa}^n$ )
$C$	tracer gas concentration (ppm)
$c_i$	surface pressure coefficient for $i$ -th surface
$D$	air permeability: flow coefficient, volumetric air flow rate, at a unit pressure difference for a specified building area ( $\text{m}^3/\text{Pa}^n\text{h}$ )
$F$	tracer gas flow ( $\text{m}^3/\text{h}$ )
$g$	acceleration due to gravity ( $\text{m}/\text{s}^2$ )
in	index: inside
$l_i$	length of the $i$ -th component (m)
lee	index: leewardside
$\dot{m}$	air mass flow ( $\text{kg}/\text{h}$ )
$n$	flow exponent, between 0.5 and 1
NPL	neutral pressure level
out	index: outside
$p$	pressure (Pa)
$Q$	volumetric air flow rate ( $\text{m}^3/\text{h}$ )
$R$	permeability ratio of a house
$t$	time (h)
$T$	temperature (K)
$V$	effective volume of the structure ( $\text{m}^3$ )

$v(10)$ or $v_{10}$	meteorological wind speed at 10 m above ground (m/s)
$v$	wind speed (m/s)
wind	index: wind or windward side
$z$	$z$ -coordinate or height of the building (m)
$z_g$	geostrophic wind height (m)
$\alpha$	exponent in the power law for the vertical wind velocity profile, depending on terrain roughness
$\Delta$	difference in conjugated item
$\rho$	density (kg/m <sup>3</sup> )
$\theta$	temperature (°C)

## REFERENCES

- P. W. O'Callaghan, *Building from Energy Conservation*, Pergamon Press, Oxford, 1978, ch. 1.
- S. M. Berman and S. D. Silverstein, *Efficient Use of Energy*, American Institute of Physics (AIP) Conf. Proc. 25, Part III, 1975, p. 247.
- R. Stogaugh and D. Yergin (eds.), *Energy Future, Report of the Energy Project at the Harvard Business School*, Random House, New York, 1979.
- W. Carnahan *et al.*, *Efficient Use of Energy*, AIP Conf. Proc. 25, Part III, 1975, Section C6, p. 81.
- H. U. Wanner, Indoor air quality and minimum ventilation, *2nd Air Infiltration Centre (AIC) Conf. Building Design for Minimum Air Infiltration*, Stockholm, 1981.
- M. Sherman, Air infiltration in buildings, Ph.D. Thesis, LBL-10712, Lawrence Berkeley Laboratory (LBL), Berkeley, 1980.
- D. K. Alexander and D. W. Etheridge, The British Gas Multicell Model for Calculating Ventilation, *ASHRAE Trans.*, 86 (II) (1980).
- H. Esdorn and W. Brinkmann, Der Lueftungs-waermebedarf von Gebaueuden unter Wind- und Auftriebseinflussen, *Gesundheits-Ingenieur*, 99 (4) (1978) 81.
- M. Hussain and B. E. Lee, An investigation of wind forces on three dimensional roughness elements in a simulated atmospheric boundary layer, *Dep. Build. Sci. Reports BS 55-57*, University of Sheffield, 1980.
- W. A. Dalgliesh, Comparison of model/full-scale wind pressures on a high-rise building, *J. Ind. Aerodynamics*, 1 (1975) 55.
- H. W. Tieleman *et al.*, A comparison of wind-tunnel and full-scale wind pressure measurements on low-rise structures, *4th Coll. Indust. Aerodynamics*, Aachen, 1980.
- J. E. Cermak, Application of fluid mechanics to wind engineering — A Freeman Scholar Lecture, *J. Fluid Engineering*, 97 (1975) 9.
- J. E. Cermak, Aerodynamics of buildings, *Ann. Rev. Fluid Mechanics*, 8 (1976) 75.
- G. T. Tamura and A. G. Wilson, Pressure difference caused by chimney effect in three high buildings, *ASHRAE Trans.*, 73 (II) (1967) 1.1.
- G. T. Tamura and A. G. Wilson, Pressure difference caused by wind on two tall buildings, *ASHRAE Trans.*, 74 (II) (1970) 170.
- H. Honma, Ventilation of dwellings and its disturbances, KTH Stockholm, *Tekniska Meddelanden*, 63 (1975).
- G. Lusch and E. Truckenbrodt, Zusammenfassende Darstellung der Untersuchungen ueber Windkrafte an Bauwerken, *Berichte aus der Bauforschung*, 41 (1964) 1.
- W. A. Dalgliesh, Experience with wind pressure measurements on a full-scale building, *Building Sci. Series*, 30 (1970) 61.
- A. G. Davenport and W. A. Dalgliesh, A preliminary appraisal of wind loading concepts of the 1970 Canadian National Building Code, *Proc. 3rd Int. Conf. Wind Effects on Buildings and Structures, Tokyo, Part 3* (1971) 441.
- C. W. Newberry *et al.*, Wind pressures on the Post Office Tower, London, *Proc. 3rd Int. Conf. Wind Effects on Buildings and Structures, Tokyo, 1971*, BRS Current Paper CP37/71.
- O. Krischer and H. Beck, Die Durchlueftung von Raemen durch Windangriff und der Waermebedarf fuer die Lueftung, *VDI-Bericht*, 18 (1957) 29.
- H. Esdorn *et al.*, Bauliche und lueftungstechnische Massnahmen gegen unerwuenschten Luftaustausch zwischen Raemen unterschiedlichen hygienischen Standards, *Final Report of the TP F2/2 of SFB 159, TU Berlin*, 1976.
- Ventilation and infiltration, *ASHRAE Handbook of Fundamentals*, 1981, Chap. 22.
- Regeln fuer die Berechnung des Waermebedarfs von Gebaueuden, DIN 4701*, 1983.
- D. T. Grimsrud *et al.*, An intercomparison of tracer gases used for air infiltration measurements, *ASHRAE Trans.*, 86 (II) (1980).
- Int. Heating and Ventilation Engineer (IHVE), Guide*, 1965.
- R. E. Bilsborrow and F. R. Fricke, Model verification of analogue infiltration predictions, *Build. Sci.*, 10 (1975) 217.
- Principles of Natural Ventilation, *BRE Digest No. 210*, Building Research Establishment, 1978.
- C. Y. Shaw and G. T. Tamura, The calculation of air infiltration rates caused by wind and stack action for tall buildings, *ASHRAE Trans.*, 83 (II) (1977) No. 2459.
- C. Y. Shaw, A method for predicting air infiltration rates for a tall building surrounded by lower structures of uniform height, *ASHRAE Trans.*, 85 (I) (1979) No. 2514.
- A. Evers *et al.*, A computer model for analyzing smoke movement in buildings, *BRE CP 69/78*, 1978.
- H. Weier, Berechnung der Stroemungsvorgaenge in mehrgeschossigen Gebaueuden, *Luft- und Kaelte-technik*, 17 (2ff) (1981) 93.

- 33 H. Feustel, Forschung im Bereich der Wohnungslueftung — Theorie vor Praxis, *Clima. Comm. Int.*, 11 (1980) 33.
- 34 G. N. Walton, Calculation of Inter-Room Air Movement for Multi-Room Building Energy Analysis, *NBSIR 81-2404*, National Bureau of Standards (NBS), 1981.
- 35 A. Macriss *et al.*, An air infiltration model for single family dwellings, *Proc. 72nd Ann. Meeting Air Pollution Control Ass., Cincinnati, Ohio, 79-14.5, 1979.*
- 36 A. Konrad *et al.*, Programmed computer model of air infiltration in small residential buildings with oil furnace, *Proc. 3rd Int. Symp. Use of Computers for Environmental Engineering related to Buildings, Banff, Alberta, 1978*, p. 637.
- 37 D. M. Sander and G. T. Tamura, Simulation of air movement in multi-storey buildings, *Paper No. 815*, Nat. Res. Council of Canada (NRCC), Div. Bldg. Res., 1974.
- 38 Private communication with Building Services Research and Information Association (BSRIA), Bracknell, UK, 1978.
- 39 A. G. Davenport, A rationale for the determination of basic design wind velocities, *J. Structural Division*, 86 (1967) 39.
- 40 H. Feustel, Schutzdruckhaltung — ein Mittel zur Reduction des aerogenen Keimtransportes, *Proc. 5th Symp. on Hospitals, Hannover, 1978.*
- 41 H. Esdorn and H. Feustel, Maschinelle und freie Lueftung von Wohngebaeuden — ein Vergleich, *Proc. XXI Int. Cong. Building Services Engineering, Berlin, 1980.*
- 42 F. Kneubuehl *et al.*, The influence of solar and thermal radiation on the energy balance of buildings, *Proc. 1st Int. Cong. Building Energy Management, Povo de Varzim, Portugal, 1980.*
- 43 R. E. Akins *et al.*, Averaged pressure coefficients for rectangular buildings, *Proc. 5th Int. Conf. Wind Engineering, Fort Collins, Colorado, Vol. 1, 1979*, p. 369.
- 44 Air flow around buildings, *ASHRAE Handbook of Fundamentals*, 1981, Chap. 14.
- 45 P. J. Jackman and B. Tech, A study of the natural ventilation of tall office buildings, *J. of Int. Heating and Ventilation Engineer*, 38 (1970) 103.